Available online at www.sciencedirect.com
ScienceDirect
Journal of Power Sources 165 (2007) 566–572
JOURNAL OF POWER SOURCES
www.elsevier.com/locate/jpowsour

Capacity and power fading mechanism identification from a commercial cell evaluation

Matthieu Dubarry, Vojtech Svoboda, Ruey Hwu, Bor Yann Liaw *

Hawaii Natural Energy Institute, University of Hawaii at Manoa, 1680 East West Road, POST 109, Honolulu, HI 96822, USA

Available online 20 November 2006

Abstract

An 18650 lithium ion cell was evaluated using dynamic stress test (DST) protocol for cycle life study. Reference performance tests were applied every 60 DST cycles to quantify capacity fade and peak power capability (PPC) degradation with cycles to the end of life. A quantitative incremental capacity analysis (ICA) was applied to identify extrinsic and intrinsic contributions to capacity fading, whereas the open circuit voltage (OCV) measurements were utilized to determine the correct state of charge (SOC) in order to accurately correlate the capacity fade with SOC. The analysis also helps us identify that cell polarization resistance change in the cycles is the primary culprit that bifurcates to both extrinsic and intrinsic origins in capacity fade and PPC degradation. This analysis allows us to develop better understanding in predicting battery performance and life in the rechargeable lithium batteries.

Keywords: Cycle life evaluation; Capacity fade; Peak power capability; Incremental capacity analysis; Polarization resistance; Life prediction

1. Introduction

Predicting battery life is a challenging subject due to the complexity of cell performance degradation. The first step to accurately predict battery life lies in the proper analysis of the degradation mechanism. Typically, characterizing capacity degradation in a battery relies on life testing using a procedure of defined protocols. This approach suffers limited applicability to any life prediction when the duty cycle is not in the same test regime. Computer modeling and simulation may have potential to overcome this limitation. The difficulty is how to construct a reliable model to predict the battery behavior and how to apply a set of useful parameters to accomplish the simulation with high fidelity. It is therefore of paramount importance to use a reliable analytical tool to derive a correct quantitative correlation of degradation rate with the state of charge (SOC) of the battery.

Here we use a 900 mAh $Li_xNi_{0.8}Co_{0.15}Al_{0.05}O_2$ (LNCAO)-based 18650 cell as a model system to illustrate how to analyze capacity fade and power capability degradation recorded in the conventional cycle life test and how to quantitatively determine various origins of contribution in the fading behavior. This LNCAO cell has been subjected to a cycle life test using a dynamic stress test (DST) schedule and reference performance test (RPT) protocols [1] according to the U.S. Advanced Battery Consortium (USABC) electric vehicle battery test procedures manual. Although these standardized procedures can quantify capacity fade in a well-defined environment, the results are not aimed to provide sufficient information regarding degradation mechanism. Some traces of degradation can be revealed by post-mortem analyses; however, the results are less quantitative, and, most importantly, the analysis offers no chronicle correlation. Barker et al. [2–4] developed electrochemical voltage spectroscopy (EVS) technique to study lithium insertion in several transition metal oxide cathode materials. We recently applied incremental capacity analysis (ICA) and close-to-equilibrium OCV (*cte*-OCV) measurements [5] to determine the correct SOC of a battery and to analyze capacity fade measured by the cycle life test protocols. In this paper, we present more detailed description of how the LNCAO cell was tested and the data analyzed to derive correlations of capacity fade and power capability degradation with cycles.

The LNCAO-related chemistry has been studied and reported in the literature [6–17]. The cell discharge curve suggests that the cell reaction is not a simple first order phase transformation in a pseudo-binary framework with a well-defined voltage plateau, even at a very low cycling rate. Moreover, the primary source of degradation comes from the positive electrode (cathode) [9]. Postmortem analyses indicate that two distinct phenomena may

* Corresponding author. Tel.: +1 808 956 2339; fax: +1 808 956 2336.
E-mail address: bliaw@hawaii.edu (B.Y. Liaw).

0378-7753/$ – see front matter © 2006 Elsevier B.V. All rights reserved.
doi:10.1016/j.jpowsour.2006.10.046

have contributed to the capacity fade. One of them is the formation of a NiO-like insulating layer (of the order of 10 nm) on the LNCAO cathode active material (CAM) primary particle surface [17], which may have contributed to the impedance increase of the positive electrode. Another one is the loss of electron conductive path on some of the CAM particles, likely due to the disconnection of carbon black with the CAM particles ("carbon retreat") [7]. We will hypothesize how the capacity fade behavior might be related to these two phenomena with a speculated chronicle correlation.

2. Experimental

The LNCAO-based 18650 cells were provided by Quallion LLC (Sylmar, CA). The positive and negative electrode compositions have been reported, for instance, in [9,10]. These cells were subjected to USABC EV battery core tests and subsequently to cycle life test with DST cycles. After each 60 DST cycles, the cell was characterized by RPT to determine its rate capacities, peak power capability (PPC), and impedance changes. We also implemented a 2-h rest period at the end of each charge and discharge regime, respectively, to determine the *cte*-OCV of the cell at the end of each regime, which was used to estimate the correct SOC.

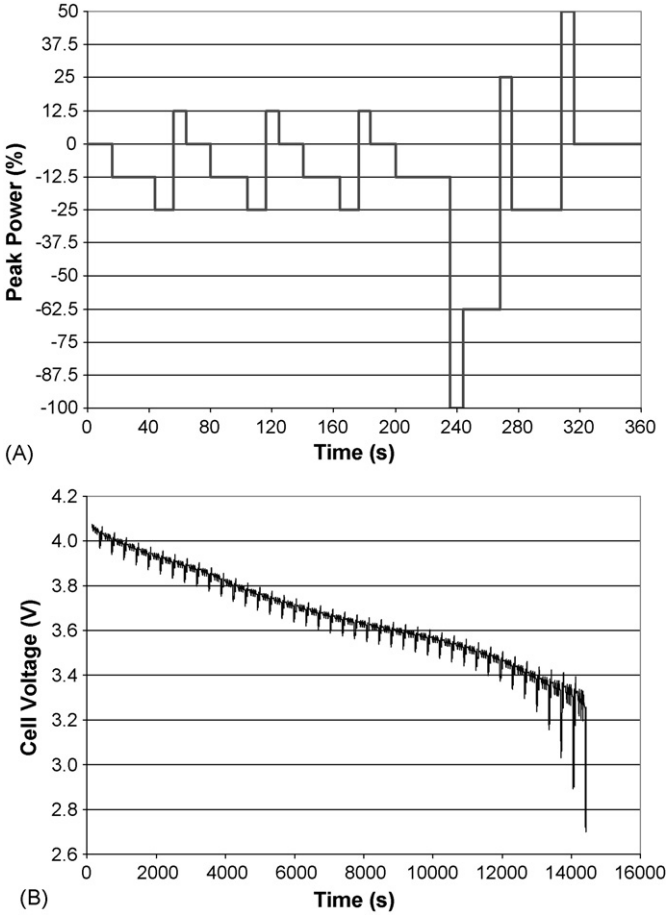

Fig. 1. (A) The DST schedule and (B) a discharge curve under the DST cycle.

The DST schedule is a series of power pulse profile mimicking regenerative braking and discharge regimens during vehicle driving for a total of 360 s (Fig. 1A). A DST cycle comprises the application of a series of DST schedules repeatedly until the cell reaches an end-of-discharge (EOD) condition (Fig. 1B) usually set off by the cell voltage that reaches the EOD voltage (EODV) cutoff. The DST cycle test was conducted using an Arbin BT-2043 battery test station with the USABC mid-term specific power goal of 150 W kg^{-1}. The cell is then fully recharged using the algorithm provided by the manufacturer, which is a two-step charge protocol beginning with a constant current (CI) regime cut off at 4.1 V, followed by a constant voltage (CV) regime until the current is less than *C*/20.

The RPT consists of three core tests: two related to the cell capacity under *C*/3 rate and constant power (CP = 2.4, 1.6 and 0.83 W, based on the specific power goal of 150 W kg^{-1}), respectively; and, one related to the SOC-dependent PPC measurements which consist of a 30-s high current ($I = 9C$) discharge step following by a low current ($I = C/10$) discharging step to adjust DOD per 10% in each step.

At the end of the cycle life test, in order to validate some hypothesis from the ICA results, we conducted additional cycle testing using a Solartron 1470 station. These additional cycles were conducted in a series of tests in which the cutoff in the charge regime was executed with a 0.05 V increment from 4.10 to 4.25 V in the end-of-charge voltage (EOCV) in each cycle to determine the respective capacity under *C*/3 rate for comparison.

3. Results

3.1. Capacity retention upon cycling: DST versus constant current regime

Before starting the cycling, four formation/condition cycles at *C*/3 were performed, and the rate capacity for each cycle was measured to be 920, 910, 912, and 913 mAh, respectively. These capacity values are slightly lower than the nominal 947 mAh at *C*/2, as determined by the manufacturer originally, but above the 900 mAh specified for this lot and model.

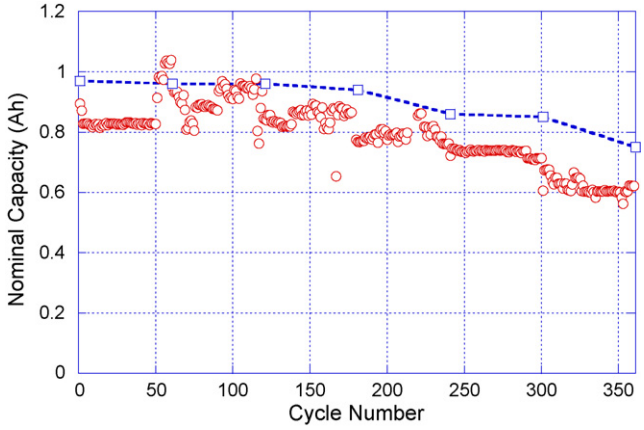

Fig. 2. Capacity retention upon DST cycle and constant current (CI) regimes. Symbols: (◯) are measured from the DST cycles and (□) are determined by RPTs at CI = *C*/3.

The cell was then cycled 361 times with DST cycles. Fig. 2 presents the evolution of the capacity with the DST cycles and the equivalent capacity determined in the RPT at CI = $C/3$ performed every 60 DST cycles, respectively. It should be noted that the regenerative braking recharge has been subtracted from the total rate capacity in every DST cycle, so the capacity presented in Fig. 2 is the net capacity. It should also be noted that the inconsistency in the capacity retention observed between 50 and 225 cycles was due to charge irregularity in the test protocol setting. As a consequence the RPT performed at the 61st cycle had not been used in the data analysis and presentation.

The capacity retention with cycle number in the DST cycling and from the RPT results at CI = $C/3$, in general, follow the same trend. We also observed that the DST cycle capacity usually was determined by the cutoff at the peak power step in the last DST schedule, as the cell voltage reached the EODV. It should be noted that the nature of this constant EODV termination usually retains capacity at the same level through DST cycling until the degradation begins to affect cell performance in a manner that the termination is triggered by other EOD conditions other than cell voltage. In this case, we shall see the capacity going through a sigmoid transition to another leveled retention. In this particular chemistry, we observed two sigmoidal transitions in the capacity retention under the DST cycling. One occurred between 225 and 250 cycles, which showed a sigmoid capacity decrease from 810 to 730 mAh, and the other between 280 and 320 cycles, exhibiting a sigmoid capacity reduction from 730 to 600 mAh.

USABC procedures define the end of life (EOL) of a battery by the condition in which the battery cannot deliver 80% of its rated capacity under a test protocol. In this case the EOL for this chemistry corresponds to about 300 DST cycles. The retention under constant current regime is expected to be more.

3.2. Power capability retention: Ragone plot and peak power test

The power capability of the cell is presented by two test protocols and representations. The first one is the construction of the Ragone plot, which reveals the specific energy versus specific power of the cell. The data used in the construction of the Ragone plot is based on the energy attainable from the cell measured at various constant power discharge cycles, typically at 25, 50, and 75% of the USABC specific power goal in W kg^{-1}. The resulting Ragone curves obtained in various RPT studies are shown in Fig. 3.

Through the first 240 DST cycles each Ragone curve displays an nearly leveled profile in the power range tested, indicating that a specific energy better than 75 Wh kg^{-1} was attainable even if the specific power went up to 60 W kg^{-1}. Beyond 300 DST cycles, however, the cell began to show noticeable power capability degradation. Although the specific energy at low power demand (e.g., 20 W kg^{-1}) was still acceptable (i.e., > 70 Wh kg^{-1}), the cell could not deliver more than 60 Wh kg^{-1} if the power demand were increased to, e.g., > 40 W kg^{-1}. After 360 DST cycles, the specific energy was again available for the specific power range tested, but the level was lower than before (~60–65 Wh kg^{-1}).

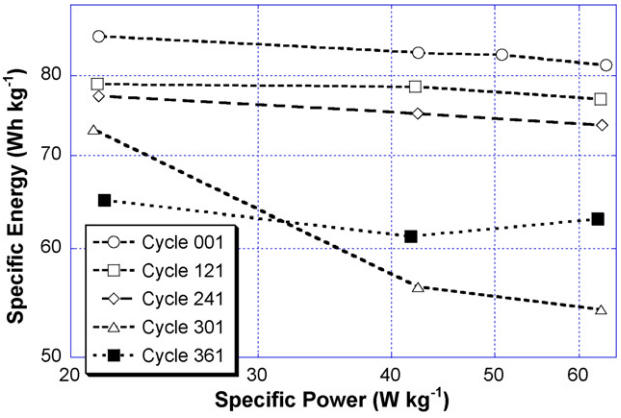

Fig. 3. Ragone plot showing the evolution of Ragone curves with cycle number.

The second representation of the power capability is depicted by the peak power capability (PPC) of a cell, as described by the ability of the battery to produce 30 s of peak power without lowering the voltage to below 2/3 of its OCV value at that DOD [1]. The evolution of PPC as a function of the DOD upon cycling is shown in Fig. 4.

As shown in Fig. 4, the PPC usually decreases with increasing DOD. For EV application the PPC at 80% DOD is a critical measure to quantify if the battery can meet the specific power demand of the USABC goal. The test results shown in Fig. 4 illustrate that the PPC degraded under DST cycling. There is a significant degradation in PPC between the 180 and 240 DST cycles. The two corresponding PPC curves showed substantially different characteristics with DOD. In order to understand the origin of this change in PPC behavior, we analyzed the cell resistance variations from the peak power test in RPTs. We estimated the polarization resistance from the following method: when the peak power pulse was imposed onto the cell, the polarization resistance was calculated from the $\Delta V/\Delta I$ measured between the base and the peak power steps. This resistance and the PPC at 0% DOD are plotted as a function of cycle number in Fig. 5. It appears that each PPC fading corresponds to an increase in cell polarization resistance. The significant loss of PPC coincides

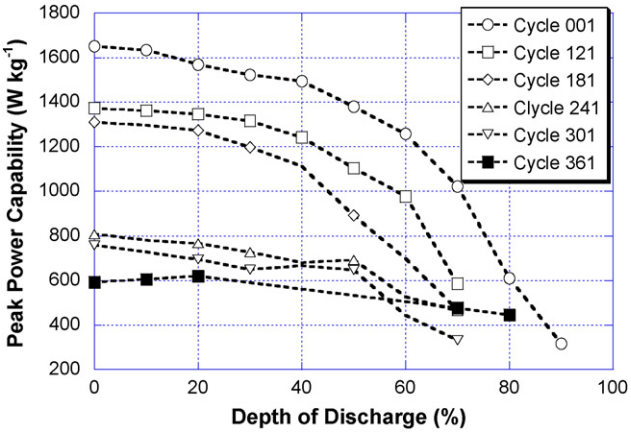

Fig. 4. Evolution of peak power capability (PPC) vs. depth of discharge (DOD) upon DST cycling.

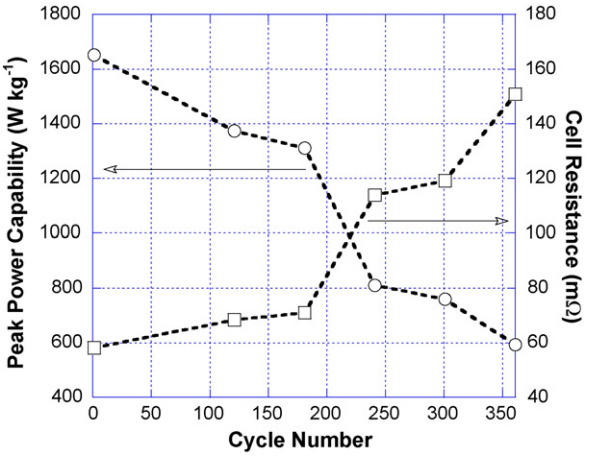

Fig. 5. Variations of PPC and cell resistance at 0% DOD over DST cycling determined by RPTs.

with a noticeable resistance increase between the two RPTs performed at the 181st and 241st cycles. This phenomenon also coincides with the change in the capacity fade shown in Fig. 6. The second jump in the cell resistance occurs between 300 and 360 DST cycles (reaching a 250% increase from the initial resistance), which also coincides with the break in trend of capacity fading as shown in Fig. 6. The correspondence therefore implies that the increase of the cell resistance is closely linked to the fading of capacity and degradation of PPC. The impact on DOD-dependent PPC is unfortunately difficult to assess due to the difficulty in executing the peak power test to the same extent of DOD through DST cycling, therefore lacking the data to provide sufficient details for comparison.

3.3. Incremental capacity analysis and cte-OCV measurements

To further understand the phenomena observed in the PPC degradation shown in Fig. 5, as well as the capacity fading observed in Fig. 2, we employed the ICA using the CI = *C*/3 data obtained in the RPTs, along with the *cte*-OCV measurements during the DST cycling. Both the ICA and *cte*-OCV techniques and their principles have been discussed in our previous work [5]. We showed that the capacity loss coincides with the increase in polarization overpotential upon DST cycling. Fig. 6a presents the evolution of the incremental capacity (IC) peaks upon cycling. There are two major IC peaks that are critical in the analysis of the capacity fade in relation to the polarization resistance increase, as revealed by (1) and (2). We noticed that as the polarization resistance at (1) increased in the cycling, as indicated by a shift of peak potential to a more positive voltage, this phenomenon results in less effective charging in the last solid solution region (>3.8 V). The reduction in the extent of the solid solution formation is evident as revealed by the discharge where the onset and range of peak (2) decreases gradually, whereas the other IC peaks remain at about the same position through the cycling. In Fig. 6b, we compare the polarization overpotential, charge input, and the capacity as determined in RPTs to reveal the association among them. Both the capacity at the 1*C* rate (◯)

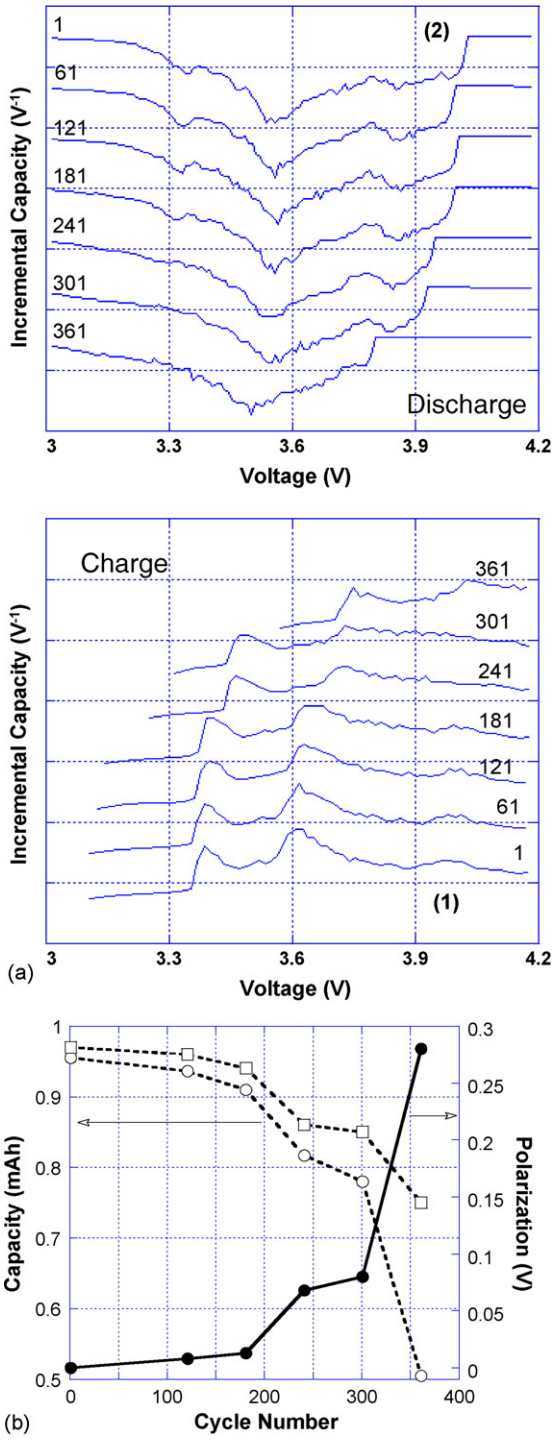

Fig. 6. (a) Evolution of incremental capacity (IC) curves and (b) capacity, charge input, and polarization overpotential upon DST cycling. Symbols: (◯) capacity from CI = 1*C*, (□) total charge input in the charge regime with the algorithm (CI = 1*C* plus CV = 4.1 V with $I < C/20$ cutoff), and (●) polarization overpotential.

and the charge input (□) using the CI–CV charging algorithm are compared with the polarization overpotential. The capacity fade and the increase in polarization are clearly linked in proportion during the first 300 cycles.

A similar correspondence can be found between the overall charge input and cell resistance up to 300 DST cycles, as shown

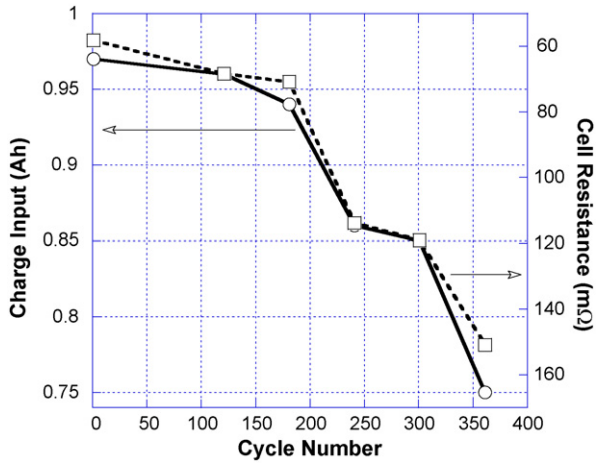

Fig. 7. Changes in the charge input (◯) and cell resistance (□) through DST cycling.

in Fig. 7. Beyond this point the two curves showed some disparity, which suggests that additional factor(s) may be affecting the degradation rate (yet to be identified), leading to an accelerated capacity fading. Interestingly, this behavior corresponds to the point where the main IC peak at 3.6 V (Fig. 6a, discharge) began to show a significant shift in the peak position. It should be noted that the progressive disappearance of the solid solution region in (2) (Fig. 6a) not only decreased the capacity but also lowered the nominal average cell voltage, therefore decreasing the PPC.

The *cte*-OCV measurements (Fig. 8a), which determine the equilibrium cell voltage at each EOC or EOD condition after a 2-h rest period, allow us to precisely determine the SOC of the cell. This technique is particularly useful in the cycle life test, when the cell degrades so the SOC cannot be monitored accurately through cycling. Indeed, upon cycling the cell voltage determined by the *cte*-OCV measurement at the EOC follows approximately the same trend as those of the cell polarization resistance and the polarization overpotential as a function of cycle number. The variation of the equilibrium cell voltage under the same EOCV after rest represents the change of SOC in the charge regime through DST cycling and it can be associated with the capacity loss. This phenomenon is denoted as "undercharging" (UC). This contribution, however, only accounts for about 17% of the capacity fade, in contrast to the 24% of total fade (Fig. 8b). Similarly, the variation of the equilibrium cell voltage under the same EODV represents the change of SOC in the discharge regime through cycling, therefore denoted as "underdischarging" (UD). In this case, UD only accounts for about 2% of fade (Fig. 8b). The remaining of the capacity fade that was not accounted for is probably attributed to either the loss of active material (LAM) in the electrode or other degradation due to side reactions with the electrolyte. Since the main IC

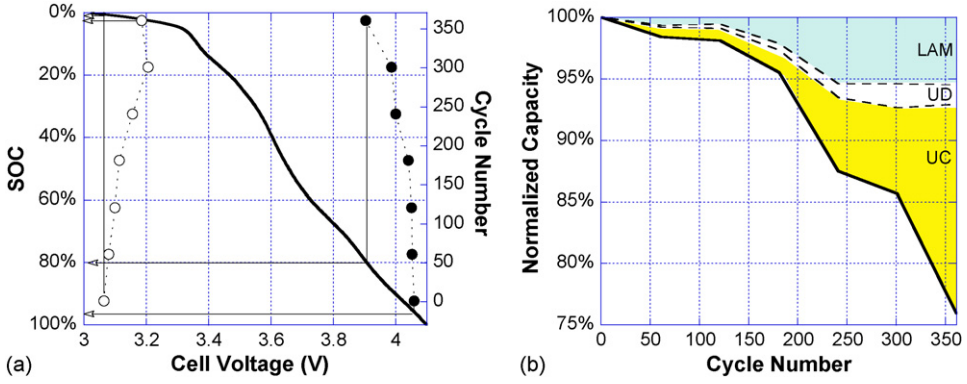

Fig. 8. (a) Evolution of *cte*-OCV of the cell in the charge and discharge regime, respectively, and (b) progression of various contributions to capacity fading through DST cycling.

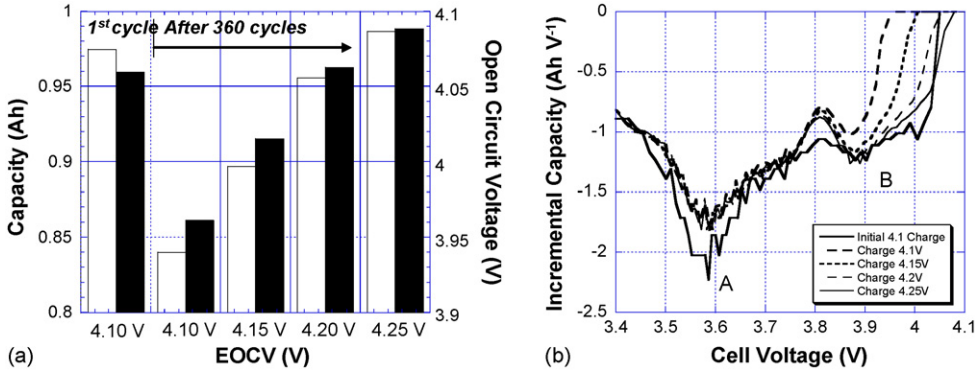

Fig. 9. (a) Evolution of *cte*-OCV (column in ■) and capacity (column in □) vs. the EOCV. The data in the first columns from the left are the result from the first cycle at the 4.1 V EOCV cutoff. The rest of the columns to the right represent those after 360 cycles with different EOCV cutoffs. (b) Evolution of the corresponding IC curves. Peak A corresponds to the first order phase transformation and peak B is related to the solid solution region.

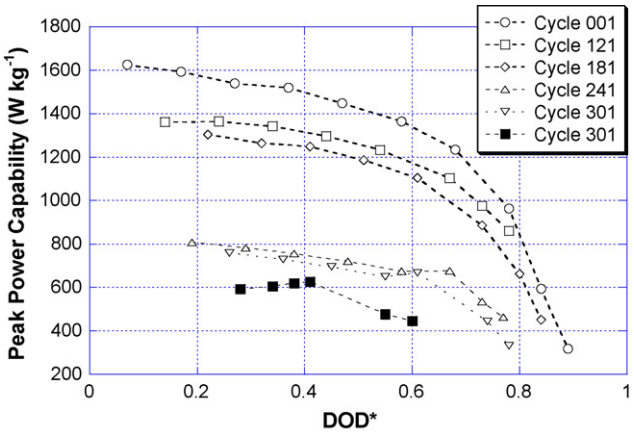

Fig. 10. Evolution of PPC vs. DOD* (corrected with SOC) upon DST cycling.

peak near 3.6 V did not shift the position on the IC curve in any noticeable manner through the first 300 DST cycles (Fig. 6a), we assume that there is no change in the chemistry (CC). Thus, it is important to note that the combined UC and UD accounts for almost 80% of the total capacity fading.

Whereas nearly 70% of the capacity fade was due to UC, we need to verify whether this capacity loss can be recovered, if the cell was terminated at a higher EOCV to offset UC. The results from the additional cycling showed that, as we raised the EOCV from 4.15 to 4.25 V with an increment of 0.05 V, the capacity and *cte*-OCV determined by *C*/3 were increased, as shown in Fig. 9a. It appears that the capacity loss due to UC can be restored; and, indeed, the *cte*-OCV at EOCV = 4.2 V is almost the same as that of the first DST cycle, indicating that the cell is reaching the same SOC, and nearly 11% out of the 17% capacity fade due to UC (upon completion of 360 cycles) have been recovered. The resulting IC curve presented in Fig. 9b shows that the integral area under the IC peak A associated with the phase transformation of the CAM was increased, as the EOCV was raised. Nonetheless, the capacity recovered was still lower than that of the first DST cycle (Fig. 9a), implying that some capacity was irreversibly lost, most likely due to the LAM. As the recovered capacity falls in the same potential range corresponding to the solid solution reaction (peak B), this capacity recovery does not appear to come from any additional capacity yielded from reactions that would occur at a higher potential, as revealed by the *cte*-OCV. Since we did not detect any significant adverse effect created by the 4.2 V cutoff either from electrolyte decomposition or other side reactions within the timeframe of the tests, we found that the cell may enjoy longer cycle life with a gradually increase in the EOCV over cycling.

The ICA and *cte*-OCV measurements show that, due to an increase in polarization, the cell was unable to recover to its fully charged state upon cycling. This result suggests that the PPC versus DOD curve presented in Fig. 4 needs to be interpreted carefully in terms of SOC. As such, we plotted the PPC in terms of a modified DOD, noted as DOD*, according to the SOC of the cell, which is shown in Fig. 10. From these results we believe that the initial fading of the PPC seems monotonic; therefore, it most likely comes from the same origin. Further degradation from cycles 181 to 241 and from cycles 301 to 361 suggest that the degradation behavior might have changed; either emerged from different mechanisms or at accelerated rates.

4. Discussion

The results from this work suggest that the capacity fade and PPC degradation are related to the change of the cell polarization resistance over cycling, since all three phenomena follow the same trend. Such a correlation also implies that they are most likely attributed to the same mechanistic origin. The nature of this origin is not well understood yet in the literature. However, with additional information reported in [6–9,14–17], we believe that a hypothesis to explain the cell degradation might be reachable. A hypothesis based on the degradation of electronic conductive path has been proposed previously by Liaw et al. [18] to speculate the cathode degradation behavior based on those reported in [6,10–12,17]. A similar hypothesis was later proposed by Kostecki and McLarnon [7]. In summary, it becomes evident that (I) both capacity fade and PPC fade are the results of the impedance growth in the cathode, (II) the CAM particles have grown with a very thin NiO-like surface composition; which is low in electronic conductivity, and (III) some carbon black lost the contact with the CAM, likely as a result of the formation of an SEI layer on the surface of the CAM particles; leading to the loss of conductive path for electrons and the disparity in SOC among the CAM particles. So, we believe that phenomena (II) and (III) indeed are associated with the increase of cathode impedance. No conclusive interpretation can be made at the present time, though, if (II) and (III) are independent or related, or if they could occur in parallel or in series. However, if (II) and (III) were independent, they most likely would run in parallel. It is possible that one takes place at a faster pace than the other to give the shape of the curve as we saw in Fig. 8b. The question is "in what order?" If (II) and (III) were dependent and related, it is likely that one occurs in consequence of the other and in series. The question of "in what order" remains.

In either case, we have two scenarios to consider. The first scenario is that the "NiO-like thin surface film formation" (II) took place first, and subsequently the "carbon retreat" (III) followed. The other is just the opposite. The shape of the trend line in Fig. 8b provides some clue for us to decipher. This capacity fade curve shows a sigmoidal transition to a temporarily steady fade before an accelerated fade taking off (likely in a power law fashion). Judging from the nature of the surface film formation (II) and the carbon retreat (III) we therefore infer that the first leg of sigmoidal transition most likely is related to the NiO-like surface film formation, while more aggressive fade in the second leg should be the result of a conductive network breakdown caused by the carbon retreat. Therefore, we can now conclude that the progression of degradation proceeds with the NiO-like surface film formation (II) first; then, the carbon retreat (III). With this understanding, we can further speculate that:

(i) If (II) and (III) were independent, the result in Fig. 8b indicates that (II) has a faster kinetics than (III).

(ii) If (II) and (III) were related and consequential, we could further hypothesize that CAM might have reacted with the electrolyte, producing the SEI layer, altering the surface composition, and leading to the NiO-like surface film formation. The formation of the SEI further broke down the carbon conductive path, resulting in the carbon retreat and the escalation of the capacity fade.

5. Conclusion

We showed that cycle life testing of rechargeable lithium battery can be used to derive useful information regarding degradation phenomena in capacity fade or power capability loss. With the aid of incremental capacity analysis and equilibrium open circuit voltage measurements we can analyze various possible attributes to the fading behavior with correct correlation with the state of charge of the cell. In this particular chemistry investigated, we found that undercharging (due to increasing polarization impedance on the cathode through cycling) contributes to the capacity fade and loss of power capability in a profound manner more than we would expect. The capacity fade due to undercharging can be recovered with proper charging control, such as increasing the EOCV to improve charge extent. Excluding undercharging and underdischarging contributions, we can begin to investigate the fading mechanisms intrinsic to the chemistry. Coupled with postmortem analysis, we can associate cathode active material degradation, such as SEI formation, surface composition change, and loss of electronic pathway, with the capacity or power fading in a chronicle manner.

Acknowledgments

This work is performed under a contract (HEVDP Contract # 46049, Supplement 5) with the Hawaii Center for Advanced Transportation Technologies (HCATT) under the support (Federal Other Transaction Agreement No. DTRS56-99-T-0017) from the U.S. Air Force Advanced Power Technology Office (APTO) at the Robins Air Force Base in Georgia. We would also like to thank Quallion LLC who provided the LNCAO 18650 cells for testing.

References

[1] Electric Vehicle Battery Test Procedures Manual, Revision 2, USABC/US DOE/INEEL, January 1996.
[2] J. Barker, R. Koksbang, M.Y. Saidi, Solid State Ionics 89 (1996) 25.
[3] J. Barker, M.Y. Saidi, R. Koksbang, Electrochim. Acta 41 (1996) 2639.
[4] J. Barker, Electrochim. Acta 40 (1995) 1603.
[5] M. Dubarry, V. Svoboda, R. Hwu, B.Y. Liaw, Electrochem. Solid-State Lett. 9 (2006) A454.
[6] X. Zhang, P.N. Ross Jr., R. Kostecki, F. Kong, S. Sloop, J.B. Kerr, K. Striebel, E.J. Cairns, F. McLarnon, J. Electrochem. Soc. 148 (2001) A463.
[7] R. Kostecki, F. McLarnon, Electrochem. Solid-State Lett. 5 (2002) A164.
[8] K.A. Striebel, J. Shim, Performance and Degradation Evaluation of Five Different Commercial Lithium Ion Cells, Lawrence Berkeley National Laboratory. Technical Report LBNL-50500. (2004) http://repositories.cdlib.org/lbnl/LBNL-50500 [Paper LBNL-50500. (2004) http://repositories.cdlib.org/lbnl/LBNL-50500].
[9] J. Shim, R. Kostecki, T. Richardson, X. Song, K.A. Striebel, J. Power Sources 112 (2002) 222.
[10] E.V. Thomas, H.L. Case, D.H. Doughty, R.G. Jungst, G. Nagasubramanian, E.P. Roth, J. Power Sources 124 (2003) 254.
[11] R.G. Jungst, G. Nagasubramanian, H.L. Case, B.Y. Liaw, A. Urbina, T.L. Paez, D.H. Doughty, J. Power Sources 119–121 (2003) 870.
[12] B.Y. Liaw, E.P. Roth, R.G. Jungst, G. Nagasubramanian, H.L. Case, D.H. Doughty, J. Power Sources 119–121 (2003) 874.
[13] H. Yang, J. Prakash, J. Electrochem. Soc. 151 (2004) A1222.
[14] D.P. Abraham, J. Liu, C.H. Chen, Y.E. Hyung, M. Stoll, N. Elsen, S. MacLaren, R. Twesten, R. Haasch, E. Sammann, I. Petrov, K. Amine, G. Henriksen, J. Power Sources 119–121 (2003) 511.
[15] R. Kostecki, F. McLarnon, Electrochem. Solid-State Lett. 7 (2004) A380.
[16] D.P. Abraham, R.D. Twesten, M. Balasubramanian, J. Kropf, D. Fischer, J. McBreen, I. Petrov, K. Amine, J. Electrochem. Soc. 150 (2003) A1450.
[17] D.P. Abraham, R.D. Twesten, M. Balasubramanian, I. Petrov, J. McBreen, K. Amine, Electrochem. Commun. 4 (2002) 620.
[18] B.Y. Liaw, R.G. Jungst, G. Nagasubramanian, H.L. Case, D.H. Doughty, Presented in the U.S. DOE Advanced Technology Development Program Quarterly Meeting at Lawrence Berkeley National Laboratory, March 13, 2002.